

ESTIMATING QUATERNARY GLACIAL EROSION IN THE ST. ELIAS MOUNTAINS, ALASKA

IAN M. NESBITT* AND WILLIAM H. KOCHTITZKY

Geodynamics Numerical Modeling Laboratory
School of Earth and Climate Sciences, University of Maine

(Dated: February 9, 2019)

ABSTRACT

The St. Elias Mountains of southeastern Alaska, one of the highest coastal mountain ranges in the world, are also home to some of the world’s highest exhumation rates. High precipitation, topographic relief, and mildly cold mean annual temperatures allow the St. Elias to host one of the largest volumes of continental, sub-arctic ice in the world. This ice comprises the remnants of the ancestral Cordilleran Ice Sheet. Understanding the landscape change caused by past and present ice masses in this region is crucial to understanding the region’s tectonic evolution. This study uses ice velocity and internal cohesive strength of geologic material to inform estimates of erosion rate and volume over two time scales that differ by two orders of magnitude. We find that glaciers account for an average of $\sim 5 \text{ mm yr}^{-1}$ of erosion in the St. Elias from 2013–2017; a value that nearly doubles during the 2013–2014 surge of Bering Glacier. Glaciers and ice sheets cause an average of 15–20 mm yr^{-1} of erosion in the region since 115 kya, and erosion nearly doubled during the last glacial maximum (LGM) ~ 18 kya. 60% of exhumation is occurring at elevations below 2000 m above mean sea level. In total, $4.3 * 10^6 \text{ km}^3$ ($\sim 1.6 \text{ km}$) has been exhumed from the orogen over the last 115 ka. We also report results from projects that used these outcomes to drive their models. Although the calculated erosion rates are corroborated by sedimentation rates in the Gulf of Alaska, spatial variance estimates of erosion could be significantly improved by using a computational method that more accurately represents the physical forces driving glacial erosion.

1. INTRODUCTION

The St. Elias Mountain Range of Alaska and western Canada (Fig. 1) is the highest coastal mountain range in the world, and has near world-record uplift rates. The region’s cool, wet climate promotes erosion that matches or exceeds uplift, and proximity of the range to the Gulf of Alaska allows for efficient removal of eroded sediment from the interior of the Yakutat terrane (Enkelmann *et al.* 2015; Gulick *et al.* 2015). Warm-based glaciers are the primary drivers of erosion in the region, covering more than 50% of the orogen (see Fig. 1). Examining the relationship between glaciers and the silicate earth in the St. Elias is essential to the understanding the interplay of forces responsible for shaping the landscape of the region.

1.1. Goals

Erosion directly links atmospheric and subsurface processes. The goal of this study is to estimate how both modern and late Quaternary glacial erosion vary over space and time. A secondary aim of the project is to provide model initialization parameters to two other groups: a silicate earth tectonophysics group, and a

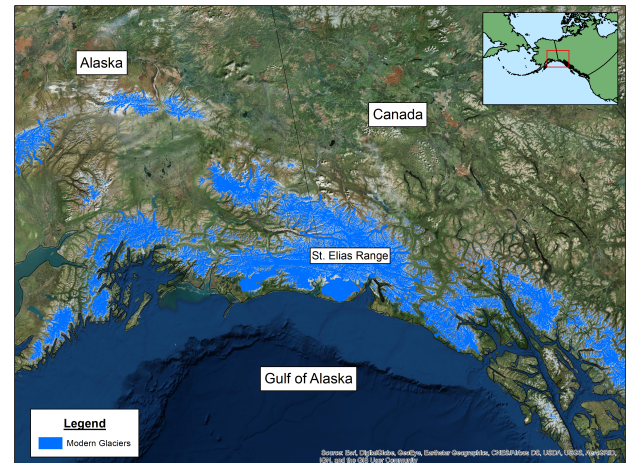


Figure 1. Satellite imagery and ocean floor hillshade of the study area, with glacial extent highlighted in blue.

group investigating the effects of glacial loading and unloading on fault locking and unlocking behavior.

Previous studies report rapid exhumation of material from the Yakutat plate (Sheaf *et al.* 2003; Spotila *et al.* 2004; Enkelmann *et al.* 2008; Berger and Spotila 2008; Enkelmann *et al.* 2009, 2015) and the coupling of atmo-

spheric, surficial, and deep earth processes in the region ([Elmore et al. 2013](#); [Enkelmann et al. 2015](#); [Gulick et al. 2015](#); [Montelli et al. 2017](#)). This study estimates glacial erosion in the region using simplified modeling methods on two timescales, in the modern era and over the last 115 kya.

Together, these three groups (tectonophysics, glacial erosion, glacial fault locking) form the basis for a unified numerical model linking tectonic forces, ice, and erosion in the St. Elias.

1.2. Tectonics

The Yakutat microplate is colliding with the North American continent at about 50 mm yr⁻¹ ([Marechal et al. 2015](#)). This collision causes significant faulting and uplift in the study area. The tectonophysics group's goal is to reproduce the uplift rates and physical features of the orogen using a 2-dimensional COMSOL model with prescribed boundary conditions informed using the outcome of this study.

This study provided the tectonophysics group a relationship of area-averaged erosion as a function of elevation in the St. Elias, which was then used as topographic control for the crust of their model.

1.3. Glacial control of seismicity

Loading and unloading of material causes changes in the internal stress and deformation of that material. Accordingly, the unloading of thick sections of glacial ice causes seismic activity in earth's crust. The glacial fault locking group's goal is to model the effect of ice loading on the frequency and magnitude of earthquakes. They hypothesize that removing thick (>1km) ice caps, such as happened during the latest Pleistocene in the Malaspina region of Alaska, causes a change in the log-log frequency-magnitude relationship of low-magnitude earthquakes. They also believe this amount of glacial unloading could hasten the release of built-up stress on locked faults, leading to the initiation of larger magnitude events.

Our aim was to provide the glacial fault locking group with *a*) ice thickness and *b*) erosion volume during the late Quaternary.

2. METHODS

We use two main datasets to estimate erosion in this study: ice velocity and material cohesion.

2.1. Ice velocity

This study uses a portion of the University of Maine Ice Sheet Model (UMISM) as the basis of ice velocity and extent to drive the long-term model ([Fastook and Chapman 1989](#); [Johnson and Fastook 2002](#); [Kleman et al. 2002](#); [Hooke and Fastook 2007](#)). UMISM estimates Cordilleran ice extent over 232 time steps during

the past 115 ka, at approximately 4 km spatial and 500 yr temporal resolution.

We also use monthly resolution ice velocity data from 2013-2017 to drive the model of modern erosion (Bas Altena, pers. comm.; [Altena et al. 2018](#)). [Altena et al. \(2018\)](#) use machine learning feature tracking software to convert Landsat 8 data at 32-day temporal resolution to monthly velocity fields.

The traditionally accepted model of velocity-driven erosion is from a study of the surge-type Variegated Glacier in Southeast Alaska in the eastern end of the study area ([Humphrey and Raymond 1994](#)). This study establishes a linear relationship between sliding speed and sediment output (1)

$$e = k * v \quad (1)$$

where e is erosion in cubic meters per time, v is velocity in meters per time, and k is dimensionless erodibility. In this model we assume k is inversely related to cohesive strength (2)

$$k = \frac{0.2}{c^t} * K_g \quad (2)$$

where c is cohesive strength in megapascals, and t and K_g are constants.

Since erosion is difficult to observe subglacially, this study must rely on fluvial erosion literature to inform the relationship between cohesive strength and erodibility beneath ice cover. Some researchers report that $t = 2$ ([Sklar and Dietrich 2001](#); [Stock et al. 2005](#)). However, since the dominant subglacial erosion mechanism is thought to be quarrying rather than abrasion (see [Iverson 2012](#); [Hooyer et al. 2012](#)), internal cohesive strength has less effect on total erosion because quarrying takes advantage of macro-scale fracture and joint orientation caused by, for example, depressurization associated with exhumation. We use $t = 0.5$, a value used in the fluvial realm ([Hanson and Simon 2001](#); [Roy et al. 2015](#)). Unlike studies conducted in regions of homogeneous rock material, southeast Alaska is a region dominated by heterogeneity. Using a lower value of t allows for a reduction of influence of internal rock strength on the model in such a region. Use of a lower value of t mutes the transition of erodibility between spatially adjacent rock strengths, and shifts the dominant influence of the model to ice velocity.

[Humphrey and Raymond \(1994\)](#) report a dimensionless, nonlinear erosion constant K_g , meant to scale erodibility to vertical distance over time. This number is generally accepted as $K_g = 10^{-4}$ m s⁻¹ ([Humphrey and Raymond 1994](#)). Several other studies (eg. [Riihimaki et al. 2005](#); [Herman et al. 2015](#)) use this constant in various glacial settings. [Riihimaki et al. \(2005\)](#) and

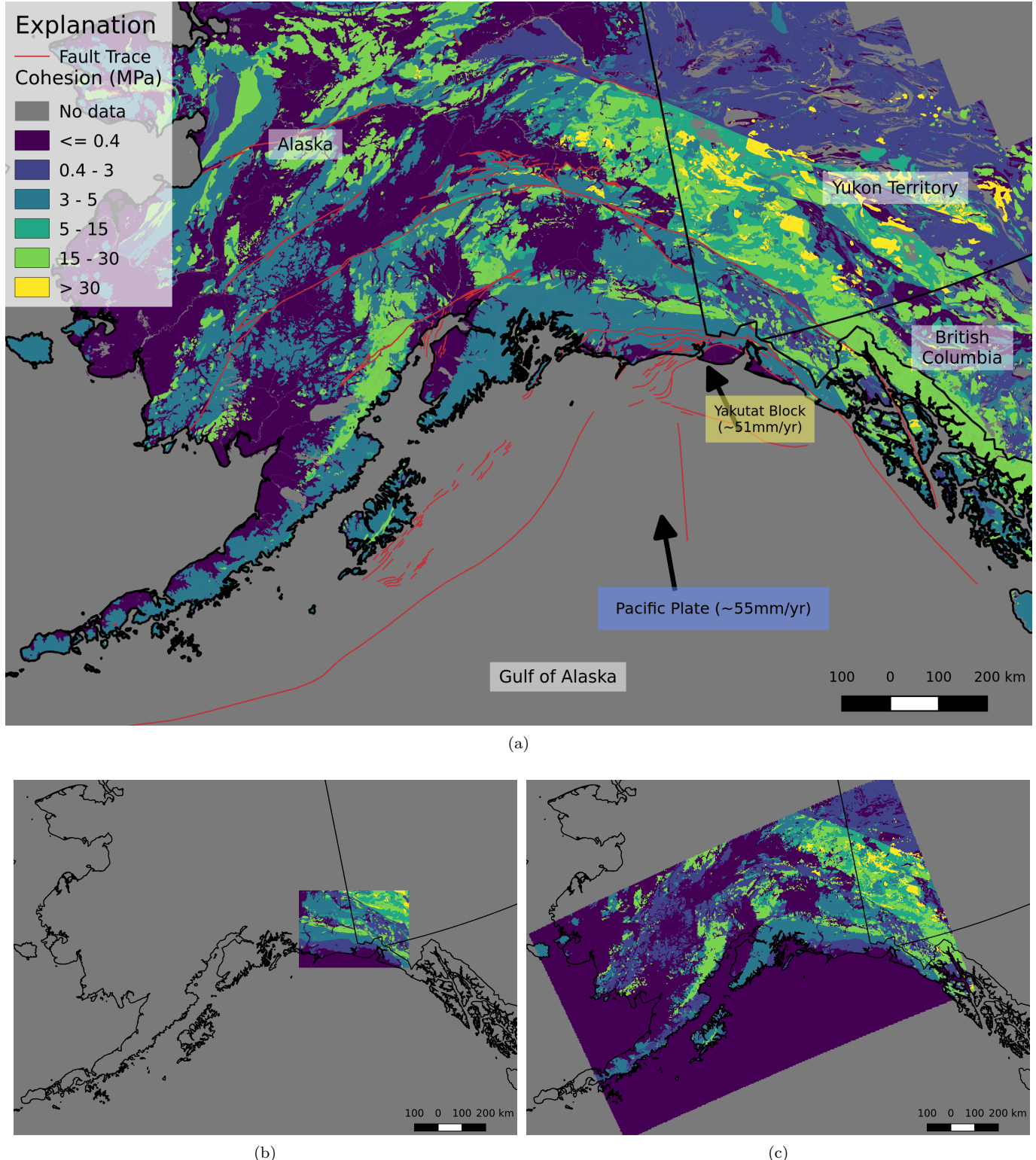


Figure 2. Modeled internal cohesion vector of geologic units in Alaska and western Canada, with (a) faults highlighted in red, and plate information and velocity specified ([Christeson et al. 2010](#); [Marechal et al. 2015](#)), (b) same data converted to extent of modern dataset at $300 \text{ m}^2 \text{ px}^{-1}$ ([Altena et al. 2018](#)), and (c) same data converted to extent of UMISM-derived dataset at approximately $4000 \text{ m}^2 \text{ px}^{-1}$ (Annie Boucher, pers. comm.). All frames in this figure are projected in Albers Equal Area conic coordinate system.

[Herman et al. \(2015\)](#) both use this value in alpine basins with homogeneous bedrock type. It is important to note that this value is a fudge factor which ignores much of the physical processes at work (see discussion in section 4.1). We choose to use this value despite our study area being much larger and more geologically complex than either of the above studies.

2.2. Assignment of cohesion values

Alaska, Yukon, and British Columbia (B.C.) all have independent geologic maps, which means when they are merged, the geologic interpretations at their borders tend to differ as often as they match up.

Table 1. Internal cohesive strength c associated with geologic designation

Map unit	Cohesive strength (MPa)
Unconsolidated deposits	0.1-0.3
Water (unmapped)	0.3
Fault gouge, 300m ² pixel	0.1 x^a
Fault gouge, 4000m ² pixel	0.9 x^b
Mudstone	0.8
Shale	1-2
Sandstone	3
Volcanic	3-5
Schist	5
Shallow intrusives	5
Marble / limestone	8-15
Unspecified metamorphics	15
Mafic / ultramafic	30
Granite / plutonic	30
Diorite	30
High-grade metamorphics	40-50
Orthogneiss	50

^aFault gouge strength in 300m² px⁻¹ cohesion model was determined by multiplying 0.1 times the strength of the parent material, x .

^bFault gouge strength in 4000m² px⁻¹ cohesion model was determined by multiplying 0.9 times the strength of the parent material, x .

References—P. Koons, pers. comm.

We merged the Alaska, British Columbia, and Yukon Territory geologic vector maps, then assigned cohesion values to certain rock types according to the strengths reported in Table 1. After value assignments, we converted vector polygons to raster using nearest neighbor

sampling for two image sizes: 461x360 for the swath of the region represented by the larger, long-term UMISM model, and 1544x1081 for the smaller, higher resolution modern model of [Altena et al. \(2018\)](#). Pixel sizes are approximately 4000m² px⁻¹ for the UMISM-derived data, and exactly 300m² px⁻¹ for the modern model (Fig. 2).

[Roy et al. \(2015\)](#) report that fractures and joints “can reduce tensile strength almost completely,” especially for brecciated fault gouge material. The results of prolonged glaciation of quaternary age fault gouges is clear in the St. Elias, where the Fairweather-Queen Charlotte fault system is nearly continuously occupied by ice fields and outlet glaciers, and accordingly these fault-adjacent areas display some of the fastest exhumation rates in the world ([Sheaf et al. 2003; Spotila et al. 2004; Enkelmann et al. 2008; Berger and Spotila 2008; Enkelmann et al. 2009; Elmore et al. 2013; Enkelmann et al. 2015](#)). To attempt to incorporate the effects of the damage zone model reported in [Roy et al. \(2015\)](#), faults in this cohesion model are treated differently based on the cell size of the cohesion raster being used (see Table 1, notes ^a and ^b). Existing cohesion values in smaller (300m²) pixels are reduced by a greater amount than in large (4000m²) pixels due to the relative area of fault damage per pixel. We assigned a value of 0.3 to areas with no data, such as beneath large water bodies. This is an attempt to estimate cohesion of both riverine floodplains and the huge amounts of Pleistocene glacial shelf sediment in the Gulf of Alaska.

We made calculations using MATLAB script for 45 modern timesteps (monthly, November 2013 - October 2017) and 232 Quaternary timesteps (115 - 0 kya in 0.5 ka steps). Outputs were saved as low-frames per second movies, color maps, and line graphics.

3. RESULTS

The two models are in general agreement on the rate and volume of erosion in the modern and recent past, to within an order of magnitude (Fig. 3, Fig. 4). The ice draining south towards the Gulf of Alaska did the vast majority of the erosive work in both models, both in terms of total volume exhumed and in rate per area. The modern model shows a greater percentage of the total erosive work being done in the north-draining watersheds than the LGM model, however this difference is within the range of modeling error.

3.1. Glacial erosion

3.1.1. Modern (2013 - 2017 CE)

This model suggests an annual mean of 5 mm yr⁻¹ (~15.5 mm total), or about 0.3 km³ yr⁻¹ (0.8 km³ total) of area-averaged erosion occurred in the 45 months covered by the dataset (Fig. 3). Of the ~0.8 km³ eroded over that time, 0.1 km³ was in north-draining water-

Erosion rate and volume by month in the St. Elias mountains

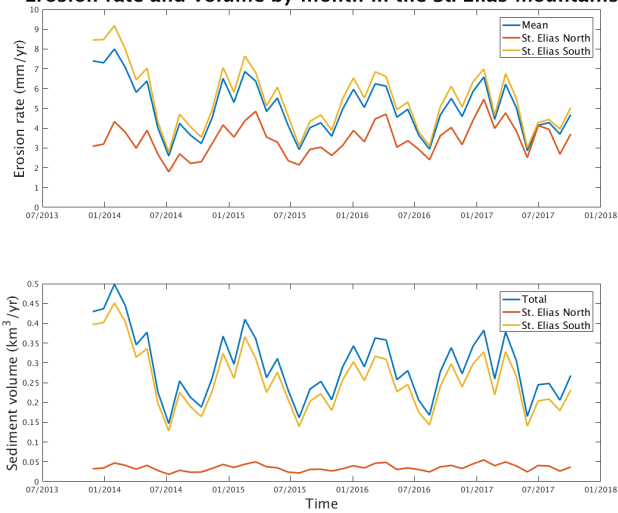


Figure 3. Monthly area-averaged erosion rate in mm yr^{-1} (top) and total eroded volume in $\text{km}^3 \text{yr}^{-1}$ (bottom) from Nov 2013 to October 2017. The effect on erosion due to seasonal change in ice velocity, and the surge of Bering Glacier in the late fall and winter of 2013 are both evident.

Erosion rate and volume in the Gulf of Alaska region

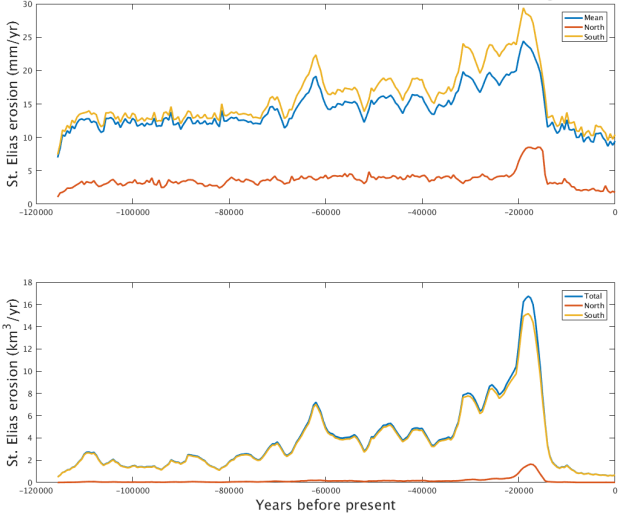


Figure 4. 500-yr mean erosion rate in mm yr^{-1} (top) and average eroded volume in $\text{km}^3 \text{yr}^{-1}$ (bottom) from 115 kya to 0 kya. Note that the vast majority of material removed by volume is from the part of the orogen that drains south to the Gulf of Alaska. The spike effect of the LGM is evident at around 18-17 kya.

sheds, and 0.7 km^3 was from areas that drain directly to the Gulf of Alaska. This suggests that the majority of glacial erosion in the region is centered on the northern part of the Yakutat block. Exhumation rate appears to vary seasonally; as ice velocity increases in the winter, so too does erosion. Additionally, specific traceable events, like the 2013-14 surge of Bering Glacier, also increase modeled erosion (Fig. 5).

3.1.2. Late Quaternary (115 - 0 kya)

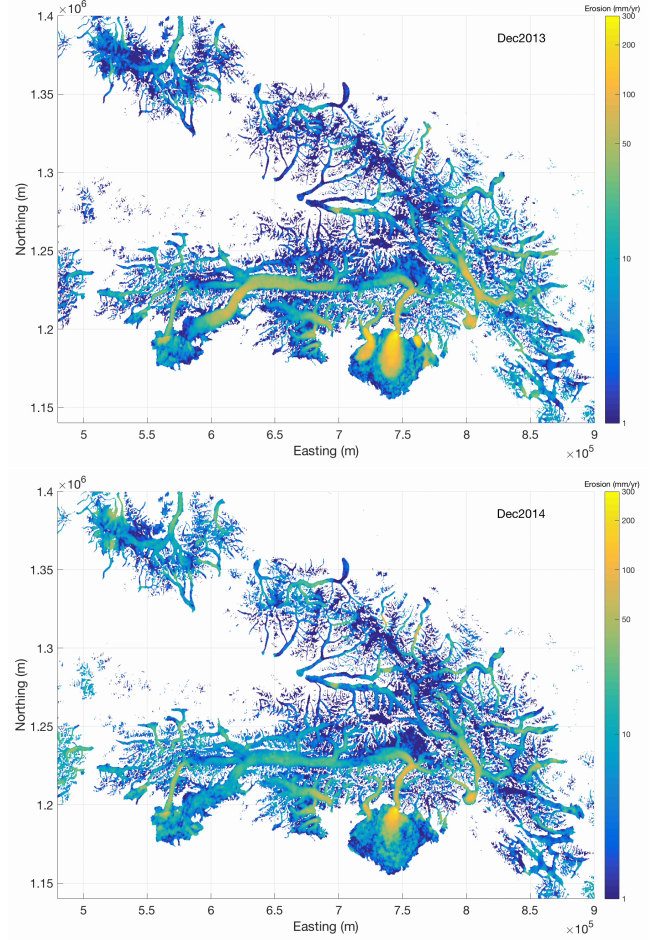


Figure 5. Log scale color map representation of instantaneous erosion rate in mm yr^{-1} in December 2013 and December 2014. Note the effect on erosion due to the surge of Bering Glacier between 6 and $7 * 10^5$ easting between 2013 and 2014.

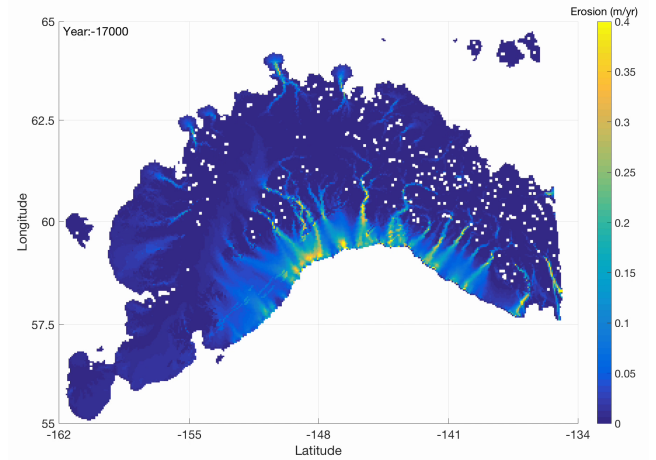


Figure 6. Linear color map of 500 yr area-averaged erosion rate in mm yr^{-1} at 17 kya, the LGM. Erosion rate is plotted on a linear scale. Erosion is concentrated in discrete ice streams which do the bulk of the erosive work in the model. All ice in the model is grounded.

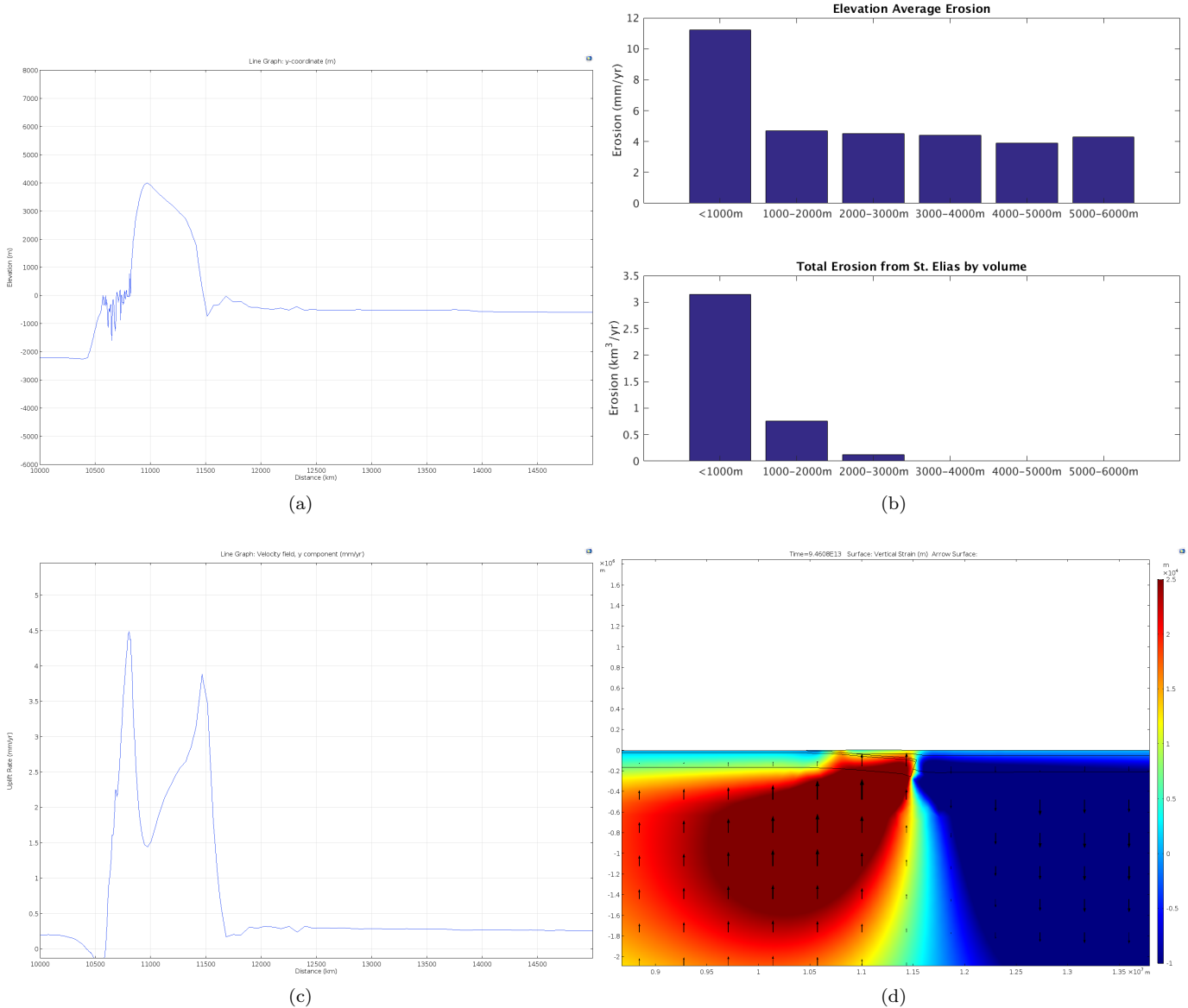


Figure 7. Results of erosion and subduction modeling plotted along a SW-NE transect across the Yakutat-North American orogen at the 3 Ma time step. Plotted here are (a) model surface elevation, (b) glacial erosion binned as a function of elevation and reported as elevation average (top) and total (bottom) per bin, (c) vertical uplift rate at the surface after erosion was applied, and (d) the vertical component of strain in color scale and arrow surface. Glacial erosion as a function of elevation is a model result of this study and a polynomial representation of the binned data represented in the top graph of (d) was used to force the tectonophysics model.

The UMISM-based erosion model suggests a mean of 14 mm yr^{-1} of area-averaged erosion occurred during the last 115 ka (Fig. 6). In total, we find that 1.6 km of area-averaged erosion ($4.3 \times 10^6 \text{ km}^3$) has occurred over the last 115 ka, a value that seems to support young fission track ages such as those found by [Berger and Spotila \(2008\)](#) and [Enkelmann et al. \(2009\)](#). Exhumation increases with ice volume, as healthy ice sheets tend to flow faster (eg. during LGM and pre-LGM events). This model shows other minor glacial maxima, such as an event at ~ 62 kya and pulses at ~ 30 kya and ~ 25

kya. The LGM time step (Fig. 6) shows erosion concentrated beneath ice streams, which terminate near the continental shelf slope.

3.2. Tectonics

Erosion in the tectonic model was forced using the results from the glacial erosion model. The tectonic modeling group found that the orogeny produced about $6 \times 10^3 \text{ m}$ of relief at the start of the model. However with erosion applied, the elevation along the inside of the orogen decreased $2 \times 10^3 \text{ m}$ over the course of 3 Ma (Fig. 7a). The erosion applied was a polynomial func-

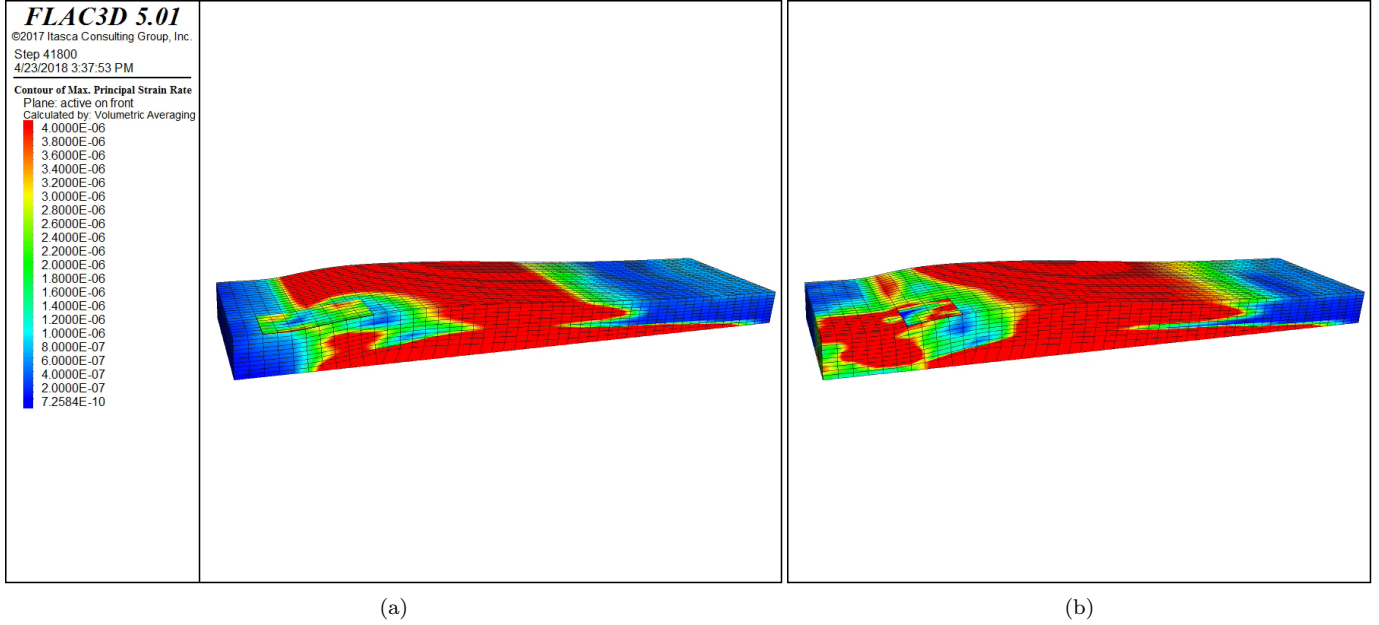


Figure 8. Modeled crustal strain beneath Malaspina Glacier region (a) before and (b) after glacial unloading. This model was sped up by six orders of magnitude to decrease processing time, therefore reported strain is 6 orders of magnitude higher in the model than in the earth's crust. Therefore, blue in this model represents $7.25 \times 10^{-16} \text{ s}^{-1}$ and red represents $4 \times 10^{-12} \text{ s}^{-1}$. Note that strain is shifted from the slope of the orogen to the forebasin after ice is removed.

tion based on the elevation average erosion calculated in this study (Fig. 7b).

The model shows that vertical strain and uplift become concentrated in two places: one just inboard of the slab hinge due to crustal shortening, and another further inland in response to slab buoying of overlying crust from below (Fig. 7c, d).

3.3. Glacial control of seismicity

Unloading ice and geologic material from the Yakutat region has the effect of altering the seismic frequency-magnitude relationship. When ice retreats, normal stress is reduced but compressive stress remains the same, which in turn allows strain rate to spike (Fig. 8). Typically, the frequency-magnitude scale is curved with a maximum at about M 1.4. However the increase in strain with the removal of ice causes an increase in both frequency and magnitude of earthquakes, centering the maximum of the frequency-magnitude slightly higher, and increasing the frequency of quakes.

Due to its higher density, unloading of earth material has a far greater control on altering strain rates in the earth's crust than unloading of ice. Since the LGM, there has been a greater mass of ice lost than earth material from the Yakutat block. Therefore any alteration in the frequency-magnitude relationship seen today is likely in response to ice removal rather than exhumation and export of earth material.

4. DISCUSSION

There is generally good agreement between erosion derived from the modeled (LGM) and measured (modern) datasets, and the models do tend to predict what we expect: that erosion is higher in higher velocity areas. This is not surprising given that we assume the mechanisms driving erosion are internal cohesion and velocity. Findings from the other groups were also positive.

The glacial fault locking group found that erosion is more effective at inducing strain than the removal of ice from the surface. Their results support the hypothesis that ice mass loss changes the frequency-magnitude relationship of seismicity in the crust. However, erosion of large volumes of material from a landscape in a short period of time must have a greater effect. The period from 30-18 kya, in which erosion averaged $\sim 25 \text{ mm yr}^{-1}$, ice sheets likely removed about 300 m of surface material from this region over the course of 12 ky, the equivalent of $\sim 0.8 \text{ km}$ of ice. This period ended at the LGM, when UMISM suggests ice mass decreased from ~ 1.2 to 0 km across the southern parts of the orogen, and 1.3 km to 0.3 km in the Malaspina piedmont region. This type of rapid unloading likely caused a spike in seismicity during and immediately following the collapse of the Cordilleran Ice Sheet. This spike in seismicity was likely made more severe by the erosion of the previous 12 ky.

The modern model shows increased erosion percentage at elevations $> 1000 \text{ m}$ compared to the UMISM model (Fig. 3b). Additionally, the modern model reports a greater percentage of erosion at high elevations $> 1000 \text{ m}$

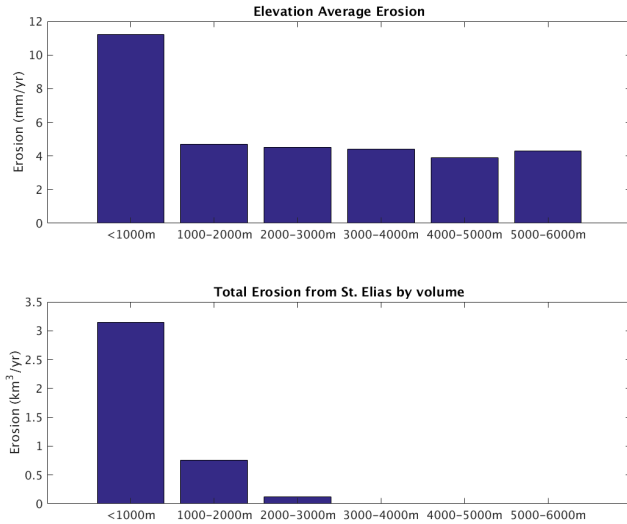


Figure 9. Average glacial erosion in the last 115 ky binned as a function of elevation and reported as elevation average (top) and total (bottom) per bin.

compared to the total volume eroded (Fig. 9). This is significant because it demonstrates the continued ability of ice to exhume the orogen as it uplifts.

Overall, we found that the orogen has been exhumed by some 1.6 km in the past 115 ky. This value is likely an underestimate, since it is averaged across the entire ice extent region. Some areas are likely to exhume much faster given ice flow through narrow troughs, and given fault zone weakness. For example, the Bagley Ice Field area and downstream Bering Glacier are positioned atop a large Quaternary-age fault zone and are likely downcutting far faster than some of the surrounding glaciers. Seward Throat, the ice stream feeding ice to the Malaspina Piedmont, exhibits some of the highest ice velocities in Alaska and according to our model is responsible for a large portion of the overall glacial erosion in the region. Locally, these two regions should display the fastest exhumation, and indeed [Berger and Spotila \(2008\)](#) suggest this may be true. However, the fact that erosion appears to be at its fastest in recent geologic time ([Spotila et al. 2004](#)) suggests that glaciation may only have initiated in the Quaternary.

According to the subduction tectonics group, the tectonic model's subducted slab appears to initiate the beginnings of tectonic aneurysm described in [Koons et al. \(2010, 2013\)](#) without the need for increased heat flow beneath the orogen (Fig. 7d). This is due to the low density ascribed to the slab to simulate young, relatively buoyant oceanic crust being subducted beyond isostatic depth (see [Clos 1993](#)).

The subduction tectonics group hypothesized that they would end up with steady-state topography prior to the end of their model run. However, the model ended up predicting the orogen losing 2 km of relief fairly

steadily over the course of 3 Ma. If we assume the elevation profile should be in approximate equilibrium over the length of the Quaternary glaciation (roughly 2 Ma), then either the subduction model is under-predicting uplift or our model is over-predicting erosion. Although we feel confident that our model is at least within range of being able to produce sediment volumes reported by geo-physical studies in the Gulf of Alaska ([Sheaf et al. 2003; Gulick et al. 2007; Boldt Love et al. 2016; Montelli et al. 2017](#)), it has important flaws and results from it should therefore be viewed with caution.

4.1. Problems

One obvious problem is reconciling geologic map data across political boundaries. Canadian geological surveys go to the trouble of interpolating bedrock type beneath glaciers, whereas the American side's glaciers are mapped as a distinct geologic unit. Our to solve this by interpolating beneath the ice ourselves is subject to order-of-magnitude scale errors. Rather than drawing straight lines from one side of the ice to the other, we tried to use evidence from topography and glacial coverage to infer underlying lithologic change. For example, where ice was obviously constricted into discretized streams we interpreted as less erodible, and where it opened into wide ice fields or piedmont, we interpreted as more susceptible to erosion.

In several places, lithologic interpretations reported on the vector maps do not align across political boundaries. We used our best judgment as to which interpretation might be correct, then manually adjusted the adjacent erroneous polygon to better reflect geologic unit continuity. Generally, these errors were associated with interpretation of surficial valley fill units in one political region versus bedrock across the border. More often than not, we revised units with less cohesive strength upward in the hopes that this would better reflect the internal strength of the underlying bedrock. However, many of these valleys could contain a considerable amount of unconsolidated material and thus interpretation of bedrock-scale cohesive strength could overestimate by a factor of 10^1 MPa or more.

However there is a more complex issue stemming from methods used in this study. Relying on velocity and erodibility to calculate erosion volume completely ignores most of the physical forces doing the work to actually erode. Equation (2) simply scales erosion per cell based on velocity using K_g . At its most basic, K_g is a linear vertical velocity used to take the place of physical modeling of material failure at the bed. Properly modeling erosion would involve calculating exceedance of critical stress at the bed and valley walls given ice flow. A better erosion model would incorporate not only internal cohesion of bedrock material but the effect of orographic

sinuosity on quarrying and abrasion near valley walls.

4.2. Future work

Although in this study the group did not have time to transition to a model that was more representative of the physical forces at work, we recommend future work focus on replicating this study using a failure earth response physics solver ([Koons et al. 2013](#)).

5. CONCLUSIONS

Regardless of the success or failure of this model to reproduce exhumation reported by other studies, it is not designed to approximate the physical forces at work at the bed and therefore incapable of physically sound ero-

sion modeling. It is a first-order approximation at best, and thus regardless of its outcome, should be improved upon in the future using finite element physics-based failure response modeling.

ACKNOWLEDGEMENTS

Profuse thanks are due to Bas Altena, who provided St. Elias glacier velocity data prior to its publication, and to Annie Boucher, who provided data from her ongoing Master's work. We would like to thank Kate, Clara, James, and Jesse, and the other inhabitants of the numerical modeling lab, for their cooperation in creating cross-informed models. Thank you also to Peter Koons, who provided cohesion data and valuable constructive criticism. Typeset using AASTEX 6.1.

REFERENCES

- Altena, B., T. Scambos, M. Fahnestock, and A. Kääb (2018), Extracting recent short-term glacier velocity evolution over Southern Alaska from a large collection of Landsat data, *The Cryosphere Discussions*, (May), 1–27, doi:10.5194/tc-2018-66.
- Berger, A. L., and J. A. Spotila (2008), Denudation and deformation in a glaciated orogenic wedge: The St. Elias orogen, Alaska, *Geology*, 36(7), 523–526, doi:10.1130/G24883A.1.
- Boldt Love, K., B. Hallet, T. L. Pratt, and S. O'Neil (2016), Observations and modeling of fjord sedimentation during the 30 year retreat of Columbia Glacier, AK, *Journal of Glaciology*, 62(234), 778–793, doi:10.1017/jog.2016.67.
- Christeson, G. L., S. P. Gulick, H. J. van Avendonk, L. L. Worthington, R. S. Reece, and T. L. Pavlis (2010), The Yakutat terrane: Dramatic change in crustal thickness across the transition fault, Alaska, *Geology*, 38(10), 895–898, doi:10.1130/G31170.1.
- Cloos, M. (1993), Lithospheric buoyancy and collisional orogenesis: Subduction of oceanic plateaus, continental margins, island arcs, spreading ridges, and seamounts, *Geological Society of America Bulletin*, 105(6), 715, doi:10.1130/0016-7606(1993)105:0715:LBACOS;2.3.CO;2.
- Elmore, C. R., S. P. S. Gulick, B. Willems, and R. Powell (2013), Seismic stratigraphic evidence for glacial expanse during glacial maxima in the Yakutat Bay Region, Gulf of Alaska, *Geochemistry, Geophysics, Geosystems*, 14(4), 1294–1311, doi:10.1002/ggge.20097.
- Enkelmann, E., J. I. Garver, and T. L. Pavlis (2008), Rapid exhumation of ice-covered rocks of the Chugach-St. Elias orogen, Southeast Alaska, *Geology*, 36(12), 915, doi:10.1130/G2252A.1.
- Enkelmann, E., P. K. Zeitler, T. L. Pavlis, J. I. Garver, and K. D. Ridgway (2009), Intense localized rock uplift and erosion in the St Elias orogen of Alaska, *Nature Geoscience*, 2(5), 360–363, doi:10.1038/ngeo502.
- Enkelmann, E., P. O. Koons, T. L. Pavlis, B. Hallet, A. Barker, J. Elliott, J. I. Garver, S. P. S. Gulick, R. M. Headley, G. L. Pavlis, K. D. Ridgway, N. Ruppert, and H. J. A. Van Avendonk (2015), Cooperation among tectonic and surface processes in the St. Elias Range, Earth's highest coastal mountains, *Geophysical Research Letters*, 42(14), 5838–5846, doi:10.1002/2015GL064727.
- Fastook, J., and J. Chapman (1989), A map-plane finite-element model: three modeling experiments, *Journal of Glaciology*, 35(119).
- Gulick, S. P., L. A. Lowe, T. L. Pavlis, J. V. Gardner, and L. A. Mayer (2007), Geophysical insights into the Transition fault debate: Propagating strike slip in response to stalling Yakutat block subduction in the Gulf of Alaska, *Geology*, 35(8), 763, doi:10.1130/G23585A.1.
- Gulick, S. P. S., J. M. Jaeger, A. C. Mix, H. Asahi, H. Bahlburg, C. L. Belanger, G. B. B. Berbel, L. Childress, E. Cowan, L. Drab, M. Forwick, A. Fukumura, S. Ge, S. Gupta, A. Kioka, S. Konno, L. J. LeVay, C. März, K. M. Matsuzaki, E. L. McClymont, C. Moy, J. Müller, A. Nakamura, T. Ojima, F. R. Ribeiro, K. D. Ridgway, O. E. Romero, A. L. Slagle, J. S. Stoner, G. St-Onge, I. Suto, M. D. Walczak, L. L. Worthington, I. Bailey, E. Enkelmann, R. Reece, and J. M. Swartz (2015), Mid-Pleistocene climate transition drives net mass loss from rapidly uplifting St. Elias Mountains, Alaska, *Proceedings of the National Academy of Sciences*, 112(49), 15,042–15,047, doi:10.1073/pnas.1512549112.
- Hanson, G. J., and A. Simon (2001), Erodibility of cohesive streambeds in the loess area of the midwestern USA, *Hydrological Processes*, 15(1), 23–38, doi:10.1002/hyp.149.
- Herman, F., O. Beyssac, M. Brughelli, S. N. Lane, S. Leprince, T. Adatte, J. Y. Y. Lin, J.-P. Avouac, and S. C. Cox (2015), Erosion by an Alpine glacier, *Science*, 350(6257), 193–195, doi:10.1126/science.aab2386.
- Hooke, R. L., and J. Fastook (2007), Thermal conditions at the bed of the Laurentide ice sheet in Maine during deglaciation: implications for esker formation, *Journal of Glaciology*, 53(183), 646–658, doi:10.3189/002214307784409243.
- Hoyer, T. S., D. Cohen, and N. R. Iverson (2012), Control of glacial quarrying by bedrock joints, *Geomorphology*, 153–154, 91–101, doi:10.1016/j.geomorph.2012.02.012.
- Humphrey, N. F., and C. F. Raymond (1994), Hydrology, erosion and sediment production in a surging glacier: Variegated Glacier, Alaska, 198283, *Journal of Glaciology*, 40(136), 539–552, doi:10.3189/S0022143000012429.
- Iverson, N. R. (2012), A theory of glacial quarrying for landscape evolution models, *Geology*, 40(8), 679–682, doi:10.1130/G33079.1.

- Johnson, J., and J. L. Fastook (2002), Northern Hemisphere glaciation and its sensitivity to basal melt water, *Quaternary International*, 95(96), 65–74, doi:10.1016/S1040-6182(02)00028-9.
- Kleman, J., J. Fastook, and A. P. Stroeve (2002), Geologically and geomorphologically constrained numerical model of Laurentide Ice Sheet inception and build-up, *Quaternary International*, 95-96, 87–98, doi:10.1016/S1040-6182(02)00030-7.
- Koons, P. O., B. P. Hooks, T. L. Pavlis, P. Upton, and A. D. Barker (2010), Three-dimensional mechanics of Yakutat convergence in the southern Alaskan plate corner, *Tectonics*, 29(4), doi:10.1029/2009TC002463.
- Koons, P. O., P. Upton, S. G. Roy, and G. E. Tucker (2013), Linking Earth and Atmosphere at Higher Frequencies with the Failure Earth Response Model, in *American Geophysical Union, Fall Meeting 2013, abstract id. EP44A-08*, San Francisco, CA.
- Marechal, A., S. Mazzotti, J. L. Elliott, J. T. Freymueller, and M. Schmidt (2015), Indentor-corner tectonics in the Yakutat-St. Elias collision constrained by GPS, *Journal of Geophysical Research: Solid Earth*, 120(5), 3897–3908, doi:10.1002/2014JB011842.
- Montelli, A., S. P. Gulick, L. L. Worthington, A. Mix, M. Davies-Walczak, S. D. Zellers, and J. M. Jaeger (2017), Late Quaternary glacial dynamics and sedimentation variability in the Bering Trough, Gulf of Alaska, *Geology*, 45(3), 251–254, doi:10.1130/G38836.1.
- Riihimaki, C. A., K. R. MacGregor, R. S. Anderson, S. P. Anderson, and M. G. Loso (2005), Sediment evacuation and glacial erosion rates at a small alpine glacier, *Journal of Geophysical Research*, 110(F3), F03,003, doi:10.1029/2004JF000189.
- Roy, S. G., P. O. Koons, P. Upton, and G. E. Tucker (2015), The influence of crustal strength fields on the patterns and rates of fluvial incision, *Journal of Geophysical Research: Earth Surface*, 120(2), 275–299, doi:10.1002/2014JF003281.
- Sheaf, M. A., L. Serpa, and T. L. Pavlis (2003), Exhumation rates in the St. Elias Mountains, Alaska, *Tectonophysics*, 367(1-2), 1–11, doi:10.1016/S0040-1951(03)00124-0.
- Sklar, L. S., and W. E. Dietrich (2001), Sediment and rock strength controls on river incision into bedrock, *Geology*, 29(12), 1087, doi:10.1130/0091-7613(2001)029;1087:SARSCO;2.0.CO;2.
- Spotila, J. A., J. T. Buscher, A. J. Meigs, and P. W. Reiners (2004), Long-term glacial erosion of active mountain belts: Example of the ChugachSt. Elias Range, Alaska, *Geology*, 32(6), 501, doi:10.1130/G20343.1.
- Stock, J. D., D. R. Montgomery, B. D. Collins, W. E. Dietrich, and L. Sklar (2005), Field measurements of incision rates following bedrock exposure: Implications for process controls on the long profiles of valleys cut by rivers and debris flows, *Geological Society of America Bulletin*, 117(1), 174, doi:10.1130/B25560.1.